Review | Vol. 10, No. 8 | 1 Aug 2019 | BIOMEDICAL OPTICS EXPRESS 4075
Biomedical Optics EXPRESS

# Review of micro-optical sectioning tomography (MOST): technology and applications for whole-brain optical imaging [Invited]

TING ZHENG,[1,2,4] ZHAO FENG,[1,2,4] XIAOJUN WANG,[1,2] TAO JIANG,[3] RUI JIN,[1,2] PEILIN ZHAO,[1,2] TING LUO,[1,2] HUI GONG,[1,2,3] QINGMING LUO,[1,2,3] AND JING YUAN[1,2,3,*]

[1]*Collaborative Innovation Center for Biomedical Engineering, Wuhan National Laboratory for Optoelectronics-Huazhong University of Science and Technology, Wuhan, Hubei 430074, China*
[2]*Britton Chance Center and MOE Key Laboratory for Biomedical Photonics, School of Engineering Sciences, Huazhong University of Science and Technology, Wuhan, Hubei 430074, China*
[3]*HUST–Suzhou Institute for Brainsmatics, JITRI Institute for Brainsmatics, Suzhou, Jiangsu 215000, China*
[4]*Equal contribution*
**yuanj@hust.edu.cn*

**Abstract:** Elucidating connectivity and functionality at the whole-brain level is one of the most challenging research goals in neuroscience. Various whole-brain optical imaging technologies with submicron lateral resolution have been developed to reveal the fine structures of brain-wide neural and vascular networks at the mesoscopic level. Among them, micro-optical sectioning tomography (MOST) is attracting increasing attention, as a variety of technological variations and solutions tailored toward different biological applications have been optimized. Here, we summarize the recent development of MOST technology in whole-brain imaging and anticipate future improvements.



## 1. Introduction

The brain is one of the most complex systems in nature, controlling all physical and mental activities. World-wide researchers have long been working on deciphering neural processes involved in memory, emotion, thought, and consciousness, along with effective prevention and treatment of brain diseases, from molecular to cellular and neural circuit level [1–6]. However, none of these have been comprehensively resolved.

Magnetic resonance imaging [7] and electron microscopy [8] have helped to elucidate the brain on the macro and micro levels. However, on the mesoscopic level [9], understanding of neurons, the basic units of brain functions and connections, and their connection map, is far from sufficient. In recent years, various research centers worldwide have implemented brain science research projects [10–12] to develop and apply a variety of novel techniques to map the connections between neurons. Among them, optical imaging technology with good spatial resolution has the natural advantage of imaging anatomical structures in the brain at the mesoscopic level. However, traditional optical microscopy techniques [13–15] only penetrate biological tissue to depths of tens or hundreds of microns because of scattering and absorption. To overcome the optical imaging depth limit and expand the imaging range from brain slices or the superficial brain area to the whole brains of rodents or higher model animals, two different strategies, clearing and mechnical sectioning had been introduced.

Two old concepts of chemical clearing [16] and light-sheet fluorescence microscopy [17] from a hundred years ago were modified, combined and modernized [18]. Various clearing techniques [19] have been developed rapidly to minimize tissue scattering and absorption and

#364298 https://doi.org/10.1364/BOE.10.004075
Journal © 2019 Received 5 Apr 2019; revised 20 Jun 2019; accepted 25 Jun 2019; published 17 Jul 2019

Biomedical Optics EXPRESS

even out the refractive index of the brain tissue. Solvent-based clearing techniques [20–22] relies on dehydration of tissue and refractive index matching by lipid solvent. Aqueous-based clearing techniques achieves homogenizing the scattering through simple immersion, hyperhydration [23,24] or hydrogel embedding [25–29]. These approach has been demonstrated to yield three-dimensional (3D) brainwide distributions of specific cells [30]. However, to the best of the authors' knowledge, no whole-morphology reconstruction of single neurons in the cleared brain has been demonstrated due to the low and inconsistent resolution of current light-sheet illumination imaging technology across the whole brain.

Optical imaging combining different histological techniques using imaging and slice alternation constitutes a new strategy towards overcoming the imaging depth limit and obtaining high-resolution images across the whole brain. Serial two-photon tomography (STP) [31], block-face serial microscopy (FAST) [32], and micro-optical sectioning tomography (MOST) [33–38] are all examples of this approach. The Mouselight platform based on STP [39] and FAST employs a vibratome to achieve the slicing process. They used a sectioning thickness of 100 μm to achieve the fastest whole-brain imaging speed of their respective systems. However, imaging the detailed morphology in the axial range of approximately 100 μm remains a considerable challenge for both systems. Although a modified clearing technique has been developed for the Mouselight platform to alleviate this problem, additional sample preparation time is required [39].

In the contrary, MOST had employed ultrathin sectioning combining line-illumination imaging on a knife edge to achieve a submicron voxel resolution for whole-brain imaging and reconstruction [33]. Then a series of MOST techniques had been developed and constituted comprehensive and quantitative experimental tools for various applications, involving neural morphology [40,41] and cell distribution [42,43], as well as analyses of neural connectomes and projectomes [36] and the microvascular network [44,45].

Here, we review current available staining and labeling methods for whole brain optical imaging, the latest developments of MOST serial technology, along with their typical applications in neuroscience. In addition, we anticipate future trends and challenges.

## 2. Sample labeling and preparation

To obtain ideal whole-brain optical imaging results, samples have to be appropriately prepared before imaging. Thus, related difficulties must be overcome, e.g successfully labeling the interested structures across the whole brain and embedding entire brains suitable for imaging remain challenging. It is difficult to observe raw brain tissue directly using optical microscopy due to the poor optical imaging contrast. Since Cajal applied Golgi silver staining to depict neuron structures more than 100 years ago [46], different staining and labeling methods have gradually been developed for visualization of different structural components, to ascertain cell populations, and to analyze neuronal and vascular anatomical connections. connections. In recent years, in particular, fluorescence labeling has greatly promoted the application of optical imaging technology in to brain science, because of its good specificity and sensitivity. However, for whole-brain optical imaging based on tissue sectioning, it is also challenging to keep the mechanical properties of the brain suitable for cutting and to maintain the brain integrity during embedding. This section presents a brief review of the labeling and sample preparation techniques that have been applied to whole-brain optical imaging. They can be used for not only MOST series technology, but also for other imaging technologies in this field.

### *2.1 Conventional staining methods*

Conventional staining methods [46–48] are typically applied to cell cultures and tissue slices, because of the slow dye penetration rate of the dye. For whole-brain optical imaging, uniform dyeing of the whole brain is required. The entire staining process such as the general scheme, the operation of each step, and selected reagents and parameters impact the final staining

Biomedical Optics EXPRESS

effect. Deep brain tissue cannot be stained well within a short penetration time, whereas superficial regions may be overstained if it takes longer penetration time. Previously, the authors' research group modified the procedure and reagents of Golgi-Cox staining protocol [49] and achieved uniform Golgi staining of intact rodent brains [33,50]. The staining time of an intact mouse brain in Cox solution was six months, which was then optimized to approximately two months. In addition, lithium hydroxide solution rather than ammonium hydroxide solution was employed to darken the intact mouse brain, so as to avoid deposition of dark substances on the knife surface during subsequent mechanical sectioning and optical imaging processes. Figure 1 shows images of layer 2–3 neurons in the primary auditory cortex in Golgi-stained two-month-old male C57 mice brains, demonstrating even staining of the dendritic arborization and dendritic spine phenotypes in the tissue. Because of strong reflection of the heavy metals, the Golgi-stained neurons are easily identified by low transmittance [Fig. 1(a)] or strong reflection [Fig. 1(b)] contrasts with the surrounding unstained tissues. Only less than 5% of neurons were randomly labeled [46], therefore, the Golgi-stained neurons could be easier identified and distinguished from the densely distributed neural networks.

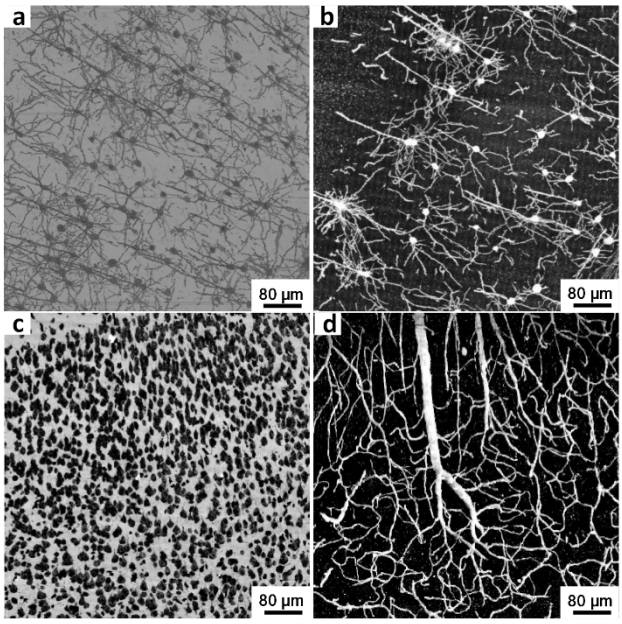


Fig. 1. Conventional staining of brain tissue. (a, b) 50-μm-thick maximum intensity projections of Golgi-stained layer 2–3 neurons in primary auditory cortex in two-month-old male C57 mouse brains, acquired via MOST and dual-mode MOST at voxel resolutions of 0.35 × 0.35 × 1 μm and 0.32 × 0.32 × 1 μm, respectively. (c, d) 100-μm-thick minimal and maximum intensity projections of the same Nissl-stained mouse brain.

Nissl staining protocol, another classical histological staining method, had been also improved for staining large-mount brain tissue [51–53]. The staining time was shortened from 1 month to 10 days by increasing the concentration and decreasing the pH value of the thionine solution in the staining step. Combined with rapid elution, this modification was conducive to achievement of a high contrast and signal-to-back ratio in the subsequent whole-brain optical imaging. This staining method allowed staining of all endoplasmic reticulum (or "Nissl bodies") [54], followed by visualization of the brain cytoarchitecture via absorption (or reflection) contrast [Fig. 1(c)]. We also observed blood vessels in a maximum intensity projection of the Nissl-stained tissue [Fig. 1(d)], thereby achieving simultaneous 3D visualization of both the cytoarchitecture and cerebral vasculature in rodent brains through

Biomedical Optics EXPRESS

whole-brain Nissl staining [44,53,55]. This modified protocol constitutes a new tool for study of cerebral circulatory pathways at anatomical landmarks. In addition, other traditional methods, such as ink perfusion had been demonstrated to stain cerebral vessles [56–59].

### *2.2 Fluorescence labeling methods*

Conventional staining methods can label structure of random neurons in circuits, but without cell type information [60]. In contrast, fluorescence molecular labeling of neurons has the advantages of good specificity and high sensitivity. In recent years, the rapid development of this technology has greatly enhanced the convenience of neurobiology research. Through combination of fluorescent labeling with optical imaging methods, more intuitive and larger-scale neuroscience research has become feasible [61,62]. In particular, fluorescence MOST (fMOST) technologies [34–37,63] have been combined with various fluorescence labeling methods to achieve tracing of different brain structures.

The most basic labeling method involves anterograde and retrograde labeling of neuronal projections using chemical fluorescent dyes. Using this technique, Zingg et al. [64] successfully constructed a cortical connectivity map of a mouse brain. Analysis of the map data suggested that the cortex subregions communicated with each other in a parallel and interactive manner. However, on a smaller scale, it is difficult to analyze the fine-structure characteristics of individual neurons and the connections between neurons using molecular probes such as fluorescent dyes.

The central nervous system is a highly heterogeneous biological system composed of a large number of neurons of various shapes, which poses great technical difficulties for cell-level research. Neuron specificity is largely determined by the genes they express; hence, it is possible to use genetics and genetic engineering techniques to analyze neuron morphology and function [65]. Molecular and genetic techniques enable to screen marker genes that are highly correlated with neuronal types and specifically expressed in a subpopulation neurons, or transcription factors that regulate the differentiation of neural stem cells and determine the fate of neurons [66,67]. For example, post-embryonic stem cell targeting and homologous recombination technology were previously employed to insert DNA-Cre recombinase or fluorescent markers at endogenous sites [68]. On this basis, various types of transgenic tool mice were developed [69,70]. These transgenic tools combining with high-resolution whole-brain fluorescence imaging provide a potential of reconstructing whole morphology of type-specific neurons (Fig. 2) and then deciphering the whole-brain connectivity.

Biomedical Optics EXPRESS

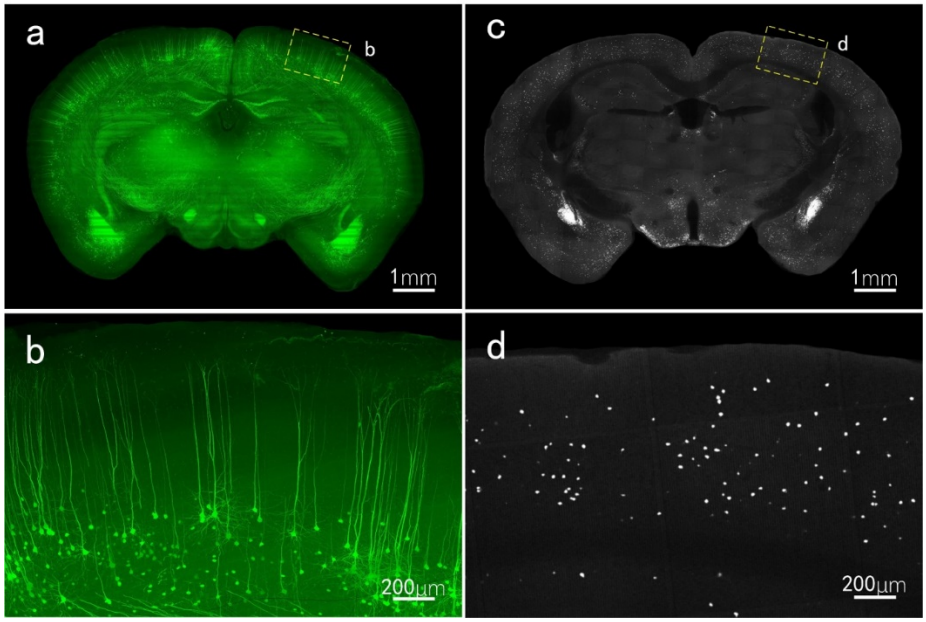


Fig. 2. Mouse brains genetically targeted for labeling. (a) Image of hippocampus coronal plane of Thy1-green fluorescent protein (GFP) mouse brain. The projection thickness is 600 μm. (b) Enlarged view of dotted box in (a). (c) Coronal images of hippocampus of SOM-IRES-Cre:Ai3-EYFP mouse brain. The projection thickness is 10 μm. (d) Enlarged view of dotted box in (c).

By transforming a neurotropic virus into a tool for nerve cell transfection, a gene containing fluorescent protein can be carried into the nervous system. Compared with non-viral neurotracers, a viral neurotracer system has the advantages of high specificity and cross-synaptic behavior [71,72]. Hence, reverse and cross-synaptic labeling of single neurons can be achieved using the infection characteristics of neurons with different virus system tools.

Fluorescence labeling of specific types of neuron can be achieved by combining a virus and the recombinase system. For example, in 2008, Kuhlman and Huang [73] used Cre-recombinase knockin mice and viral-mediated gene transfection technology to mark inhibitory neurons having various functions in the mouse brain; hence, preliminarily analysis of the morphological characteristics of these neurons was performed.

Sparse and high-brightness labeling can also be achieved using viral and molecular techniques. Recently, Lin and colleagues [41] developed a sparsely highlighted single-neuron virus labeling strategy which, combined with fMOST imaging, can accurately analyze the complete morphology of a single neuron. Figures 3(a) and (b) show that this strategy can yield the whole-brain output of a single excitatory neuron in the somatosensory cortex (S2) in mice, with long-range projection terminals and their fine structures being clearly apparent.

By exploiting the retrograde transsynaptic transmission of the rabies virus, single synaptic connection labeling of specific types of neuron in the whole brain can be achieved [74,75]. Figures 3(c) and (d) show the input across single synapse on the whole-brain scale and the vertebral neurons in the S2 brain region obtained by combining rabies virus markers with fMOST imaging, respectively.

In addition to the structural connection, molecular phenotypes of neurons and neural circuits are also important for understanding cell types and circuit functions. The developments of chemical clearing technology have provided an important pathway to immunostain tissue blocks. Various chemical clearing techniques had demonstrated the images of different immunostained organs and tissue by light sheet illumination microscopy [20,21,23–27]. It is not suitable for sectioning due to the change of tissue characteristics after

Biomedical Optics EXPRESS

clearing treatment. Therefore, address this challenge is important for improving compatibility of whole-mount immunostaining with the sectioning-based whole brain optical imaging methods.

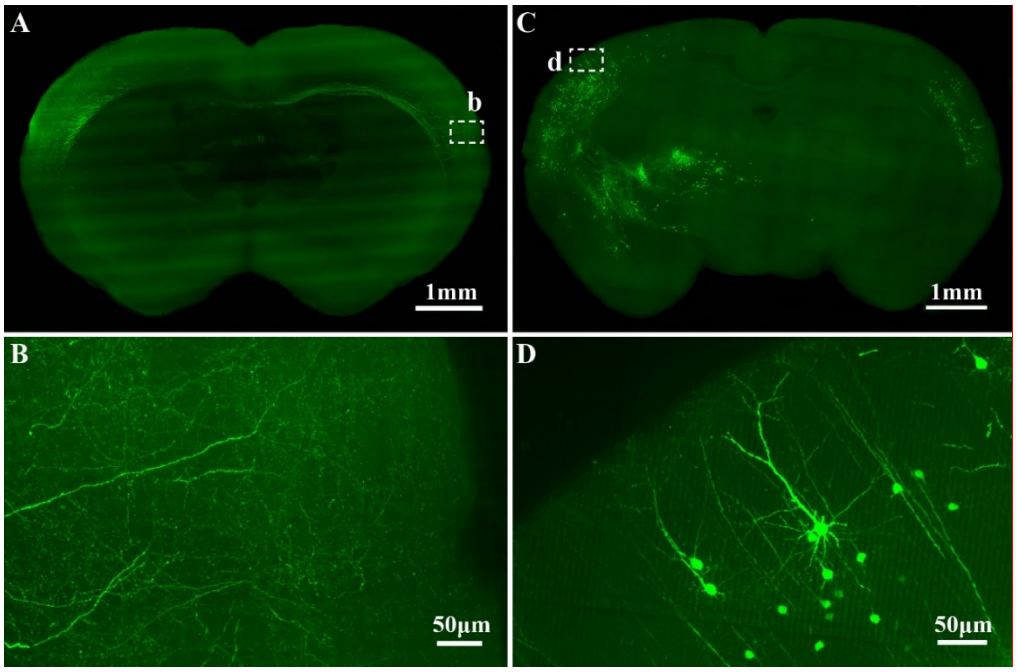


Fig. 3. Virus-labeled input and output of Thy1 pyramidal neurons in somatosensory cortex (S2) area of mouse brain. (a) Thy1 pyramidal neuron output in S2 near injection site and (b) details of projected nerve fibers on opposite side of injection site. (c) Input distribution of Thy1 pyramidal neurons in S2 in hippocampus coronal plane and (d) enlarged view of white dotted box in (c).

Accurate localization of the neural structure is a prerequisite for accurate identification of the spatial composition of the whole-brain neural structure. We have also proposed the concept of real-time counterstaining [36]; this approach avoids additional whole-brain staining to provide cellular architecture localization assistance to obtain 3D information of interest. Real-time cytoarchitecture counterstaining is a simple, flexible, and easy whole-brain staining method because no additional sample preparation is required. The low permeability cytostructured dye is used to achieve real-time counterstaining of the sample surface instead of the whole brain. This strategy also avoids potential background interference from the deep tissue. Furthermore, the cutting–staining–imaging cycle ensures consistent staining effects across all imaged surfaces. By this approach [36], fluorescent-labeled neurons in the same field of view were imaged simultaneously with the cytoarchitecture, without additional time costs for acquisition of anatomical location information or further registration of different channels. This concept can also be extended to other whole-brain optical imaging methods based on mechanical cutting, such as the series of STP and fMOST systems.

In addition, our previous work has shown that a low-temperature environment can effectively enhance the quantum efficiency of fluorescence [76]. Therefore, we have also successfully detected the endogenous fluorescence of senile plaques in a liquid nitrogen environment [63]. The obtained model indicates that the cryo-imaging environment provides a potential means of label-free observation of specific features and expands the scope of whole-brain 3D imaging objects.

Biomedical Optics EXPRESS

### 2.3 Intact-brain fixation and embedding

To determine the inter-neuron connection network at the whole-brain level of mice, it is necessary to fix the network during sample pretreatment. Fixation can prevent autolysis during specimen preparation to avoid possible changes of the fine-structure morphology of tissue, enabling to withstand long-term whole-brain data collection. Currently, there are two commonly tissue fixation: immersion soaking [77–79] and perfusion [18,80–82]. Immersion soaking fixation involves long-term immersion of fresh tissue in fixative solution [20,81,83]. The perfusion fixation method is used in both the STP [31] and MOST series of systems [33] to achieve complete fixation of the whole-brain tissue. Currently, there are four types of fixative: 1) aldehydes: paraformaldehyde and glutaraldehyde [83]; 2) oxidants: osmium tetroxide, potassium permanganate, etc [84,85]; 3) alcohols: methanol, ethanol, etc [86]; and 4) others: mercury chloride, picric acid, etc [87]. Aldehyde fixative is most conducive to maintaining the fluorescence intensity, but has a slightly poor fixation effect on micro structures [84,88]. Among them, 4% paraformaldehyde is the most commonly used solution [89–91], followed by a fixative mixed with different proportions of glutaraldehyde or picric acid [92,93].

Because of the limited imaging depth of optical methods, in traditional histological techniques, samples are usually sliced for observation of microscopic details. Researchers have developed a variety of sample embedding methods suitable for different slicing techniques, including paraffin, collodion, resin, and agar embedding. The paraffin and collodion embedding is most widely used [94,95] while quenches fluorescent proteins and increases autofluorescence [96,97]. In 2012, STP [31] used agar instead of paraffin to reduce the effect of the embedding process on the tissue fluorescence. However, as agarose cannot penetrate tissue effectively, a sample section thickness of tens of microns as required and the imaging plane surface could only be positioned tens of microns below the sample surface. Therefore, ideal high-resolution imaging results cannot be obtained using single-photon imaging and this embedding method. Even two-photon imaging requires additional clearing to overcome the tissue scattering interference and other factors affecting the deep tissue imaging quality [39]. Comparatively, with reference to resin plastic embedding technology used in electron microscopy [98], our group embedded polymer in biological tissue to increase its hardness [99]. Hence, combining with optical imaging, we had achieved a high-quality data acquisition over the whole brain at submicron voxel resolution. For Golgi staining [Fig. 4(a)] and Nissl staining [Fig. 4(c)] samples, spur resin embedding was used. while GMA [Fig. 4(b)] or HM20 [Fig. 4(d)] resin embedding was used for fluorescence labeling samples. We found that the fluorescence was weakened by protonation in the resin embedding process. To overcome this problem, we employed an alkali solution to immerse the sample during imaging and found that the fluorescencecould be effectively reactivated, thereby obtaining the ideal imaging effect. For samples subjected to a low-temperature imaging environment, a mixture of glycerol, anhydrous ethanol, and deionized water was used as the embedding agent.

Biomedical Optics EXPRESS

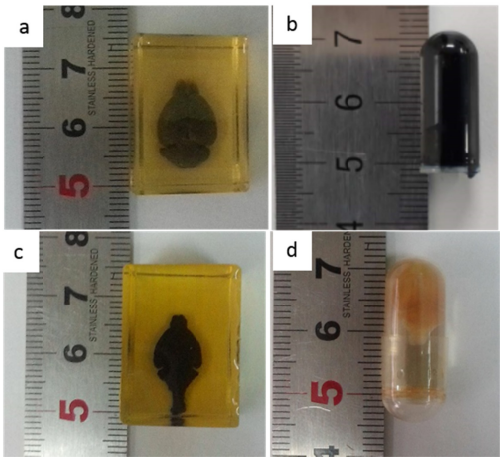


Fig. 4. Resin-embedded mice brains .Golgi-stained mouse brains (a) in Spurr resin. (c) Nissl-stained mouse brain in Spurr resin. Fluorescence-labeled mouse brain in GMA resin (b) and HM20 resin (d).

## 3. Technical development of MOST

To obtain an optical tomographic image of a complete rodent brain of several centimeters in size, a number of parameters, such as the resolution, imaging range, imaging time, system robustness, automatic image registration, and cost have to be considered and balanced. Based on different optical imaging principles, various types of recently developed whole-brain micro-optical imaging technology have allowed development of a variety of effective schemes for analysis of whole-brain spatial information according to specific research needs [100].

### *3.1 Technical requirements for whole-brain optical imaging*

The brain structure is extremely complex, leading to a number of technical challenges for whole-brain micro-optical imaging at the mesoscopic level. The size of cell bodies and arteriovenous blood vessels may reach up to dozens of microns, whereas the diameters of neuronal fibers and capillaries are in the submicron to several-micron range. The diameters of axon boutons, dendritic spines, and synapses are even less than 1 micron. On the other hand, for brains, for example, of mice or rats, the imaging range should reach more than 1 cm in three dimensions. Therefore, to decipher fine structures in the brain (i.e., cell bodies, blood vessels, nerve fibers), consistent high-resolution imaging across the whole brain must be achieved.

The whole-brain optical imaging time is the time required to traverse the imaging range, which is determined by the imaging resolution, imaging range, and scanning mode. The larger the numerical aperture, the higher the resolution, but the longer the time required to traverse the entire sample. The time of whole-brain optical imaging by existing technologies ranges from a few hours (with low resolution) [31,32] to a few days (with high resolution) [34,36,39] at different resolutions. For biological experiments requiring statistical studies, whole-brain optical imaging has to balance imaging throughput and resolution to achieve large-scale data acquisition. On one hand, appropriate resolutions should be selected for different research objects to shorten the acquisition time. On the other hand, new imaging methods are expected to improve lateral and axial scanning strategies to achieve higher imaging speeds.

Automatic registration of tomographic images in whole-brain imaging is also a great challenge. High-resolution whole-brain data sets are extremely large, with typical file sizes of terabyte order [36,39]. Tomographic image registration through later image processing only is

Biomedical Optics EXPRESS

very complex and time-consuming. Thus, automatic registration of tomographic images in imaging schemes would greatly reduce the difficulty of the subsequent data processing.

Achievement of a high signal-to-noise ratio (SNR)/signal-to-back ratio is another important technical problem to be solved in the context of whole-brain optical imaging. Even with high resolution, ideal imaging results cannot be obtained when the SNR is insufficient. High SNR can be achieved in several ways, such as through design of an improved labeling strategy for enhanced signal intensity, along with improvement of the sample processing and embedding scheme to reduce background fluorescence (in the case of fluorescence imaging). For imaging systems, especially fluorescence imaging systems, a optical sectioning effect that reduces background interference through use of appropriate methods is necessary, such as confocal and light sheet illumination.

Another technical challenge that is often neglected pertains to the imaging system stability. As a complex opto-electromechanical integrated system, a whole-brain optical imaging system has high requirements regarding high-frequency use, uninterrupted operation, and high anti-interference capability during rapid imaging. For example, wide-field large-volume tomography system (WVT) is used to collect a whole-brain data set for mice, the camera captures more than 1 million photographs [36]. This large data volume generates high stability requirements that must be considered during engineering-based design and implementation of the system.

In whole-brain optical imaging, the imaging parameters of the imaging system should be flexibly adjustable according to different requirements, i.e., the physical size of the target structure and the neurobiological application. The optical and voxel resolutions of the imaging system have a significant impact on the imaging results. If either of these resolutions fails to meet requirements, inaccuracies will appear in the imaged structure. Generally speaking, the optical resolution is required to be equivalent to the size of the structure to be observed. A voxel resolution of less than half the optical resolution will yield a well-resolved structure observation. In Table 1, recommended imaging parameters for common structures are given based on the authors' experience. Reaching or exceeding the recommended parameters will yield image data suitable for the desired application.

**Table 1. Recommended whole-brain optical imaging techniques and parameters for different applications in brain science ($R_{op}$ and $R_{vo}$: optical and voxel resolutions, respectively)**

| Structures of interest | Research goals | $R_{op}$ (μm) | $R_{vo}$ (μm$^3$) | Technology |
|---|---|---|---|---|
| Synapse-associated protein | Synaptic morphological analysis | ~0.15 | 0.08 × 0.08 × 0.1 | Spinning disk confocal microscopy (on slice) [1] |
| Dendrite spine & bouton | Dendrite spine/bouton morphology & quantitative statistics | ~0.3 × 0.3 × 1 | 0.2 × 0.2 × 1 | fMOST [36] |
| | Morphology tracing of densely distributed neurons | | | fMOST [101] |
| Morphological segmentation of axon, dendrite, capillary, and neuron soma | Topological reconstruction of long-projection axons | ~0.5 × 0.5 × 2.5 | 0.5 × 0.5 × 2 | fMOST [34,36], STP [39] |
| | Dendritic topological reconstruction | | | fMOST [34,36], STP [39] |
| | Soma morphology segmentation | | | fMOST [42,43] |
| | Capillary network | | | fMOST [45] |
| Cell counting, arteriolae, and venules | Cell counting | ~2 × 2 × 5 | 2 × 2 × 3 | fMOST [42,43], light-sheet microscopy [32,102,103] |
| | Arteriolae and venules | | | fMOST, light-sheet microscopy [22] |

Biomedical Optics EXPRESS

Synapse-related structures are very small and electron microscopy is commonly used for their imaging [104]. If an optical microscope is used, the lateral resolution must reach the diffraction limit of the optical microscope and the voxel resolution must be within 100 nm. The results reported to date have been limited to slice imaging [105,106], because the high time cost prevents achievement of whole-brain imaging [106]. To quantitatively count the dendritic spines or axon boutons which are approximately 1 micron in size, a voxel resolution of up to 0. 2 × 0. 2 × 1 $\mu m^3$ should be reached. For reconstruction of dense structures such as interneurons, the same level of imaging parameters are also needed. To date, only MOST technology has successfully achieved the required level for whole-brain imaging [101]. Axon long-range projection tracking, dendritic topology reconstruction, cellular morphological segmentation, and capillary network mapping require similar resolutions. In particular, axon long-range projection tracking is currently a popular research topic in the field of whole-brain imaging, and results from various whole-brain imaging systems have been reported [34,36,39]. Imaging of the fatty tissue capillary network using light-sheet illumination microscopy combined with optical clearing technology has been demonstrated [22]; however, for whole-brain capillary imaging, only MOST technology has yielded relevant results to date [45]. Microvessels and capillaries have sizes exceeding 10 microns. The cell-body counting and positioning requirements are relatively low. In general, lateral and voxel resolutions of approximately 2 and 3 microns, respectively, can satisfy the requirements of this imaging application. Many whole-brain imaging systems have shown similar results [30,32,107].

### *3.2 MOST technology*

Combination of slicing and imaging offers the potential to achieve consistent high resolution across the whole brain; this is the concept adopted for MOST technology. For the first-generation MOST technique [33], a method of simultaneous slicing and imaging was adopted, and a diamond knife was used to perform continuous slicing of resin-embedded mouse brain samples with 1-μm thickness. The ultra-thin brain slices formed on the blade were imaged via line scanning. Data was obtained in a layer-by-layer manner until the whole brain was imaged. Taking the diamond knife as the substrate, high-contrast absorption imaging of ultra-thin slices was realized through epi-illumination, to achieve better association with traditional dyeing methods. As the tissue section thickness was less than the optical diffraction limit, the axial resolution was the section thickness. The lateral resolution was determined by the optical imaging configuration. Using this technique combined with the improved Golgi staining method, a whole-brain Golgi-staining data set for mice with a voxel resolution of 0.35 × 0.35 × 1 $\mu m^3$ was obtained for the first time [33]. Subsequently, a Nissl-stained whole-brain sample was imaged, and a 3D data set of the whole-brain cellular architecture and vascular network of mice was obtained [53]. The arteriovenous and capillary networks were successfully distinguished [45]. Imaging on the knife edge had been demonstrated by McCormick et al. [108]. The illumination approach by a knife-collimator assembly in their system led to increasing the complexity and decreasing the stability of adjustment devices, further easily causing chatter. In contrast, the first-generation MOST addressed these issues by decoupling the illumination and cutting to make physical sectioning more easily free of chatter.

The rapid development of fluorescence labeling technology has furthered development of new versions of MOST technology. Different from absorption imaging, when fluorescence labeling is applied, the excitation light can excite the out-of-focus sample tissue under the knife surface to generate a strong background fluorescence interference. To overcome this problem, a slit was added in front of the detector to generate a confocal effect at the image position of the knife surface; hence a high-resolution fluorescence whole-brain imaging was achieved [34]. In the same study, non-inertial scanning based on the principle of the acousto-optic effect combined with continuous motion of the 3D translation stage was used to realize

Biomedical Optics EXPRESS

rapid and stable scanning of mouse whole brains. Using this method, long-range projection tracing of a single neuron axon was achieved for the first time [34,100].

In the above techniques, slicing and imaging are performed simultaneously on the knife surface. Although the axial resolution is improved, the quality requirements for sample embedding and slicing are very high. To reduce the system debugging complexity, the present authors' research group developed the two-photon fMOST (2p-fMOST) [35] system, which incorporates separate imaging and slicing processes. Optical section imaging of the surface of the sample block is performed; then, the imaged tissue is removed. This method greatly reduces the dependence of the imaging quality on the cutting quality and further improves the system stability. To effectively eliminate background interference from undersurface tissue, two-photon excitation imaging was applied to obtain the ideal tomography effect. Different with STP [31], this system still employed resin embedding and diamond sectioning for continuous axial sampling. Point-by-point scanning is still too slow for mouse brain samples with a 3D span of several centimeters, having an imaging time of more than 200 h. Therefore, exploration of more rapid imaging methods is necessary.

In 2016, we achieved a WVT system [36] to improve imaging throughput. This technique employs the wide-field imaging method of structured illumination and mosaic scanning to complete acquisition of dual-color whole-brain data within 3 days with a voxel resolution reaching $0.325 \times 0.325 \times 2\ \mu m^3$. In addition, in combination with a real-time counterstaining method, a brain-wide positioning system (BPS) was created to annotate the anatomical orientation information of the structure of interest at single-cell positioning precision. On this basis, we employed a three-window and two-color dichroic mirror to modify the system for Golgi-stained whole-brain samples [38].

Neurobiological research not only focuses on acquisition of structural information, but also aims to facilitate relevant biochemical analysis to obtain higher-dimensional information. To this end, we combined a vibratome with WVT [37]. The resultant device not only controlled the whole-brain imaging time to within a few hours via axial interval sampling, but also fully automatically collected all sections for subsequent immunohistochemical staining or sequencing of the sections of interest.

In addition to effective detection of the fluorescence signals of internal markers, our research group also studied effective enhancement of fluorescence signal intensity in a low-temperature environment. Hence, we developed cryo-MOST [63], and for the first time observed the 3D distribution of senile plaques in mouse whole brains through detection of their autofluorescence. Thus, a new tool for study of Alzheimer's disease (AD) through unlabeled imaging was developed.

Apart from the fluorescence background signal from outside the focal plane, the autofluorescence of biological tissue also interferes with imaging quality during imaging of large samples of biological tissue. The autofluorescence of biological tissue, and especially animal tissue, is very complex. Lipofuscin, collagen, etc., produce autofluorescence when stimulated by light, which interferes with the target signal. The aldehyde group carried by the aldehyde reagent used to fix samples during histological treatment also reacts with the amino acids or proteins in the tissue to form a new fluorescent substance, increasing the background fluorescence. To solve this problem, we not only considered different optical tomography principles to obtain images with high signal-to-back ratios, but also employed Sudan black B (SBB) in the sample embedding to reduce the background fluorescence [109,110]. Hence, the imaging quality of the fluorescence-labeled samples was further improved. SBB is a lipid soluble lysochrome diazo dye with strong light absorption characteristics in the visible spectral range. Because of this property, SBB can easily penetrate brain tissue with organic solvents and bind to lipids in the tissue. Experimental results have shown that this method is effective for further background suppression.

Biomedical Optics EXPRESS

## 4. Applications

Comprehensive characterization of neuronal cell types, their distributions, and connectivity patterns is critical for understanding the properties of neural circuits and their behavior generation mechanisms. Using MOST technology, researchers can study a biological process in the context of its 3D environment, identify rare events in large tissue volumes, and trace cells and cell–cell interactions over large distances. In this section, various applications of MOST technology are presented and discussed.

### *4.1 Cytoarchitecture for brain organization and neuron compartments*

Understanding the organization of the brain and its neuronal compartments is crucial for neuroscience research. One of the most fundamental requirements is a method of capturing the cytoarchitecture of the brain tissue. A whole-brain cytoarchitecture map can also provide a standard atlas for revealing the basic characteristics of certain brain areas or subareas.

In conjunction with the MOST system, we have used Nissl and propidium iodide (PI) staining methods to acquire 3D mouse and rat whole-brain atlases [36,53]. The Nissl staining results could provide brains of a variety of animal species with a standard reference atlas for areal landmarks identification [53]. The PI staining can be conducted in real-time when performing fMOST imaging in resin-embedded samples labeled with green or yellow fluorescent protein (GFP or YFP, respectively) [36] (Fig. 5). Thus, in our previous studies, Nissl-like cytoarchitecture information for quantitative analysis was successfully obtained for each imaged brain. Moreover, as Nissl staining of large whole-mount samples has limited feasibility, PI staining combined with the BPS imaging may provide an alternative and readily method for mapping brain cytoarchitectonic atlases of primates specimens.

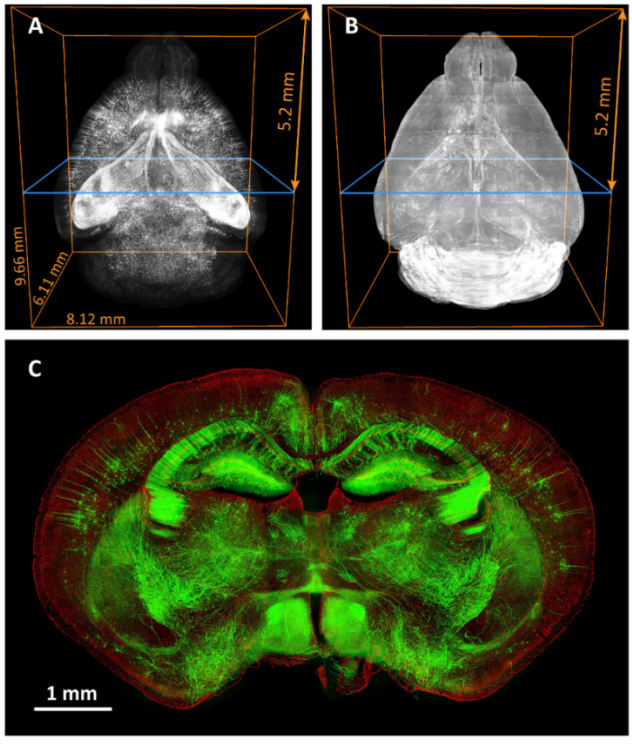


Fig. 5. Visualization of Thy1-GFP mouse brain using fMOST. (a) Top view of GFP expression. (b) Top view of propidium iodide (PI)-counterstained cytoarchitecture. (c) Merged images of GFP-labeled neurons (green) and PI-stained cells (red).

Biomedical Optics EXPRESS

### 4.2 Quantitative distributions of specific neuron types

Brain cells are composed of diverse genetic-specific neuron types. Each neuron type, with high probability, plays distinct connectivity and functional role in the brain network, and usually possesses specific cell areal distributions and unique anatomic features, such as the soma shape. Our serial of fMOST systems can feasibly image the whole-brain distributions of specific cell types [42,43].

Through combination with transgenic Cre mouse lines and reporter lines, we have used fMOST system to map the brain-wide cell distributions of genetic-specific neuron types [42,43]. By employing the NeuronGPS tool [111] for automatic soma detection and the self-registered cytoarchitecture atlas obtained via PI staining, quantitative cell distribution data could be achieved in 3D on the whole-brain level. Figure 6 shows the brain-wide distribution patterns of CRH-positive neurons across different areas and subareas. The distribution maps of other genetic-specific neuron types of interest can also be acquired through the same method.

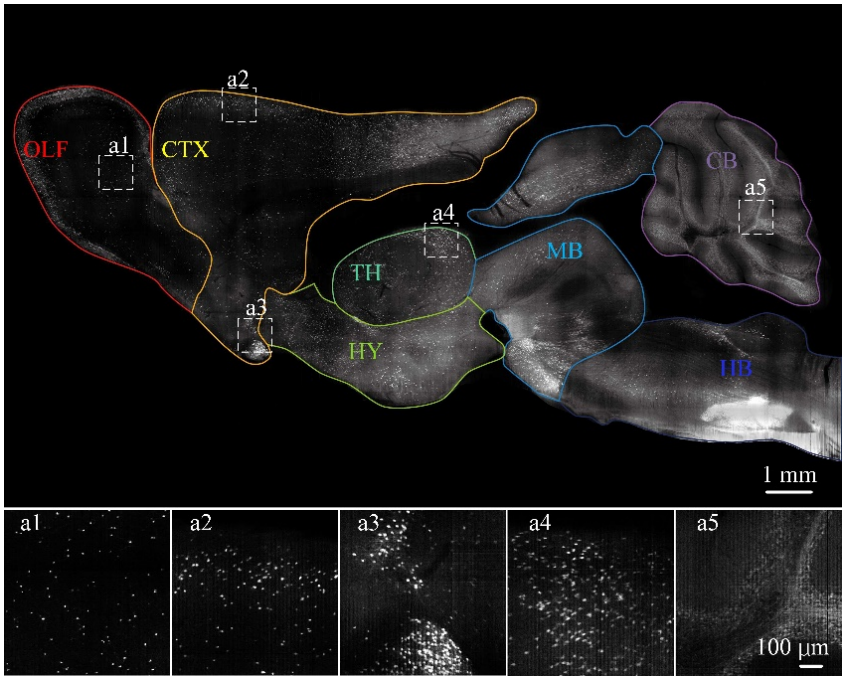


Fig. 6. Sagittal reconstruction of maximum intensity projections of CRH-IRES-Cre:Ai3-EYFP mouse brain. The projection thickness is 100 μm. (a1)–(a5) Enlarged views of white square boxes in sagittal image. The dimensions of (a1)–(a5) are 496 × 496 × 100 $\mu m^3$.

### 4.3 Brain long-range projectomes

Imaging the long-range projections among brain areas is one of the most substantial goals of brain connectivity research [47]. The resultant maps can reflect the pathways and targets of information transfer in the brain.

The fMOST series of systems can map neural circuits across different areas (Fig. 7). By combining anterograde adeno-associated virus (AAV) labeling and the fMOST whole-brain imaging, neuron projection patterns of distinct brain areas can be feasibly achieved [36]. Figure 7 shows the overall neuron axonal fiber distributions of the ventral tegmental area (VTA) in the mouse brain. This study describes the region-level connectivity or gross projections in different regions of VTA neurons. In future, systematic mapping of the

Biomedical Optics EXPRESS

projecting patterns of specific function-related brain areas will further facilitate our understanding of the brain circuit connection and function mechanisms.

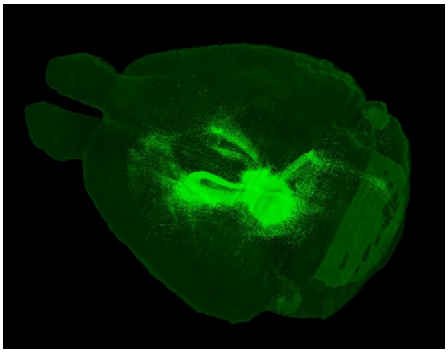

Fig. 7. Dorsal view of 3D reconstruction of brain-wide projection labeled with AAV vectors expressing GFP and imaged by 2p-fMOST.

### *4.4 Complete single neuron morphology on brain-wide scale*

Single neurons are the basic composing units of the brain network and can be classified into diverse neuron types based on their different molecular, functional, and connecting features. Morphology is one of the most intuitive depictions of neurons that reflects their input-output connectivity; therefore, the imaging, characterization, and quantification of their complete and fine structures at single-neuron level will greatly facilitate our identification and classification of anatomic neuron types. Anatomic neuron types can be described by their location, morphology, and connectivity.

To this end, fMOST techniques have enabled imaging and reconstruction of the complete morphology of single neurons, whether long-range projection neurons [34] or complex-morphology interneurons [101]. With subcellular imaging resolution, the single-neuron axons of sparsely labeled fluorescent samples over the brain-wide space can be discriminated and completely traced (Fig. 8). Further systematic and quantitative study of single-neuron projecting targets and fiber distribution patterns of molecularly or physiologically specific neurons will potentially provide an ultimate, perfectly structured wiring map for the brain network.

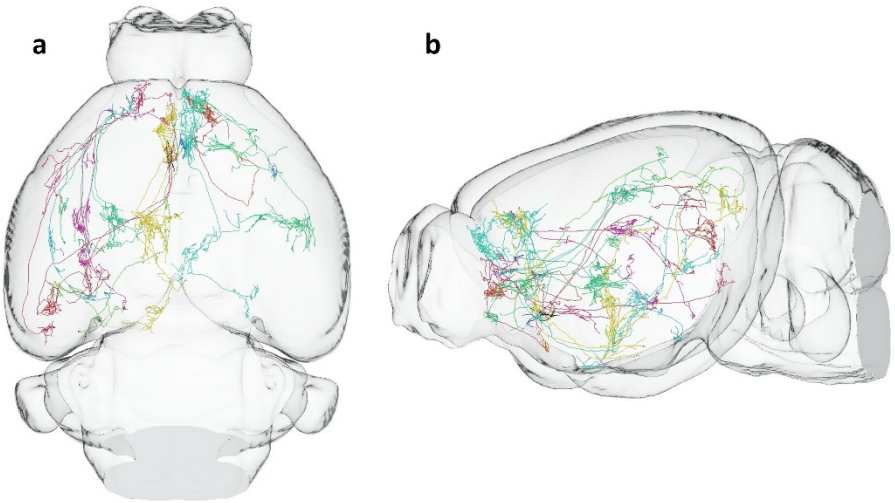


Fig. 8. Morphological reconstructions of individual pyramidal neurons. Different colors represent different cells: (a) top view, (b) sagittal view.

Biomedical Optics EXPRESS

### 4.5 Molecular identification of neural individuals

For neuron circuit investigation, multiple kinds of information are needed simultaneously. To facilitate various whole-brain labeling and imaging schemes, researchers are eager to combine morphological, distribution, and molecular phenotype information to achieve a thorough understanding of the specific neurons. Various whole-mount immunostaining techniques [20,26,27,29] may satisfy requirements to some extent; however, their reliability is limited by the need for extra-long-term tissue treatment. Moreover, the cost of a large amount of antibodies is too high. Therefore, we designed an automatic slice collecting device [37]. The high efficiency of this device enables selection of fluorescent-positive slices for subsequent immunostaining to capture native molecular information, such as c-Fos expressions, or to obtain gene expression information through in situ experiments. Figure 9 shows the workflow for whole-brain cell distribution mapping of c-Fos expression changes after electric foot shock stress modeling [112]. Significant changes are apparent in the lateral septal nucleus, bed nucleus of the stria terminalis, medial preoptic nucleus, paraventricular hypothalamic nucleus, and central amygdaloid nucleus areas. As only the slice of interest is selected for immunostaining, the staining difficulties and sample treatment time and costs are greatly reduced.

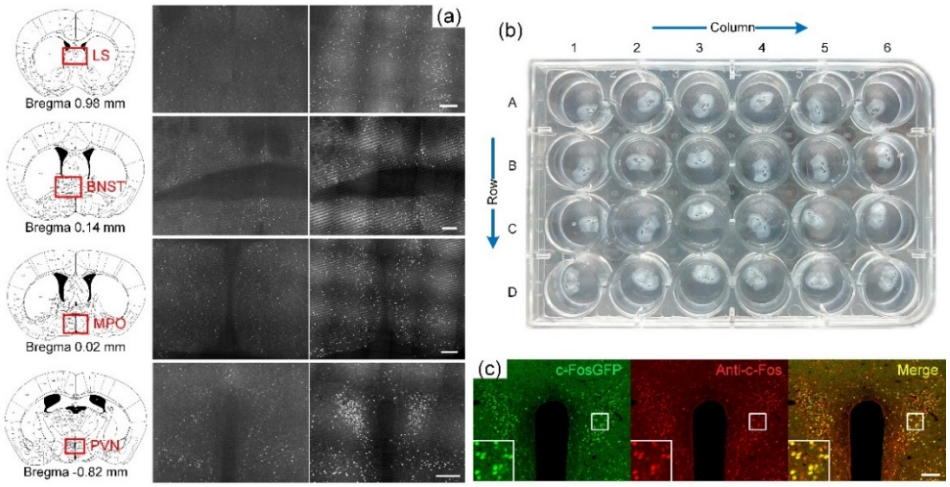


Fig. 9. c-Fos expression changes after foot shock stress modeling. (a) Significant changes in c-Fos expression levels in main brain areas. The middle and right columns show the groups without and with foot shock treatment, respectively. The left column shows the corresponding brain areas. Brain areas: LS, lateral septal nucleus, BNST, bed nucleus of the stria terminalis, MPO, medial preoptic nucleus, PVN, paraventricular hypothalamic nucleus, CEA, central amygdaloid nucleus (b) Automatic storage of imaged tissue slices in perforated plate. (c) Anti-c-Fos immunostaining result for paraventricular hypothalamic nucleus. The scale bars in (a) and (c) are 200 and 100 μm, respectively.

### 4.6 Blood vascular network

The brain is an organ rich in blood vessels, and a quarter of the body's total oxygen consumption is used to maintain nerve activity. Common brain diseases, such as stroke, AD, and tumors, are also accompanied by abnormal cerebral vascular structures. Cerebral blood vessels are characterized by tortuosity and changeability, and blood vessels are usually interlaced with each other; thus, a 3D image is required to represent the complex vascular anatomy.

The authors' research group has established a technical system for acquisition, processing, and analysis of cerebrovascular data based on five mouse whole-brain data sets obtained via MOST (about 10,000 coronal surfaces were collected in each brain and the total data set of

Biomedical Optics EXPRESS

the five brains had a size of about 10 TB) [44,45]. Detailed cerebrovascular maps spanning the brain were constructed, including arteries, veins, arterioles, and venules (Fig. 10). This study not only reconstructed the whole vascular network in three dimensions, but also used the cytoarchitecture of the same mouse brain to realize stereotactic localization of the vascular branch starting points at single-cell level. With the aid of high-resolution vascular reconstruction data, many previously unreported venous branches were found and named according to the common naming rules. Further quantitative analysis of the connectivity and blood supply relationship between arterial and venous vessels and brain regions will facilitate intuitive understanding of arterial blood transport to specific brain regions/nuclear groups through specific vascular branches, and collection and gathering of venous blood after energy supply. The constructed atlas will constitute an important basic resource database for study of brain functions and disease.

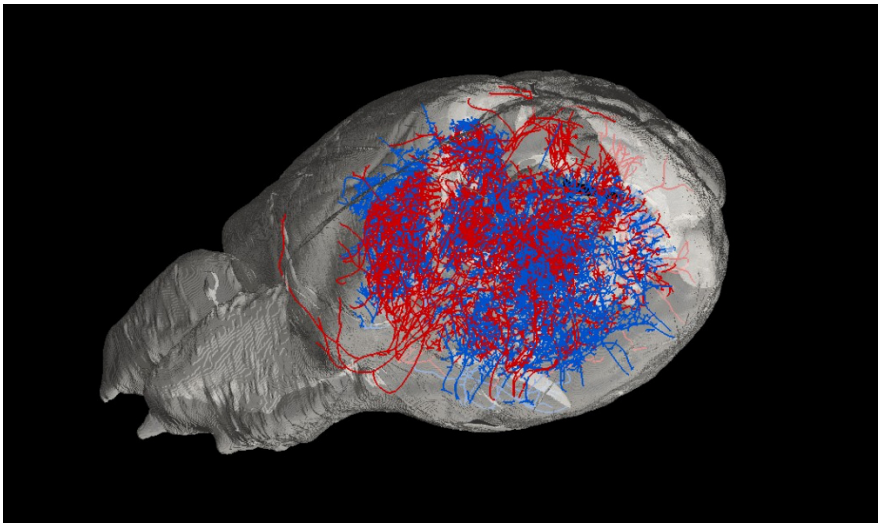

Fig. 10. Dorsalateral view of vascular network in Nissl-stained mouse brain. Red and blue represent arterial and venous networks, respectively.

### *4.7 Label-free visualization of Alzheimer's pathology distribution*

Neurological and psychiatric diseases usually induce brain-wide changes. Among them, AD causes production of amyloid plaques that change their shapes and distributions with pathological evolution.

Using the endogenous fluorescence contrast provided by senile plaques, Luo et al. [63] developed a cryo-MOST method that realized label-free optical imaging of senile plaques in transgenic AD mouse brains. Label-free brain-wide visualization of Alzheimer's pathology distributions and morphologies may be useful for quantitative study of neurodegenerative disease mechanisms and for drug efficacy evaluation. Figure 11 shows the coronal distributions of amyloid plaques in the hippocampus. Compared to the work of Whitesell et al. [113], in which methoxy-X04 injections were employed for amyloid plaque labeling, the cryo-MOST method could provide more realistic and objective results showing the overall distributions and shapes of amyloid plaques in the brain. Furthermore, sample cryo-fixation is simple and easy, with no sample deformation, in contrast with chemical fixation methods.

Biomedical Optics EXPRESS

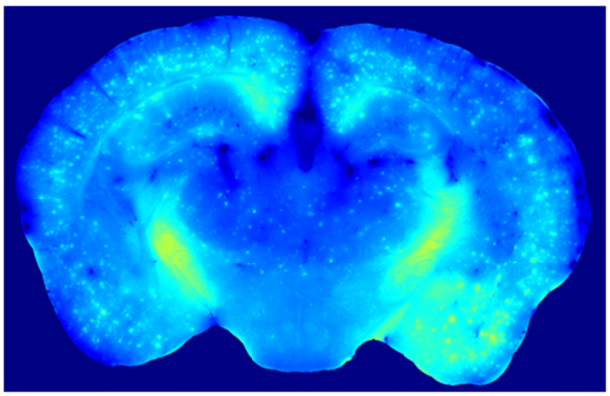

Fig. 11. Senile plaque distribution in hippocampus acquired by cryo-MOST.

## 5. Future challenges and prospects

Whole-brain optical imaging technology has developed rapidly in recent years and has demonstrated its application potential in the field of brain science, e.g., in cell-type classification [6], connectomics, and projectomics. Unprecedented 3D information of the whole brain has been acquired, providing a new, informative, and illuminating perspective on the brain. The intense interest of neuroscientists in this new research tool has motivated consideration of how best to develop whole-brain optical imaging. Acquisition of a complete set of whole-brain 3D data sets is not a simple imaging problem, as effective combination of whole-brain sample labeling, embedding, and mass image data processing technology is required. Therefore, to better develop and promote whole-brain optical imaging technology, procedures include sample preparation, optical imaging, and image processing should be simultaneously enhanced.

Development of sample labeling methods with better specificity, controllable expression, and stronger signals is important for improved quality of images derived from signal sources. For sample preparation, embedding technology with small deformation, good cross-linking, and good tissue support must be developed. In addition, it is important to maintain the biochemical characteristics of the biological tissue during sample preparation, to allow subsequent application with histological analyses of genes and molecules. Development of more efficient 3D traversal methods, improvement of imaging throughput and speed, and shortening of the whole-brain 3D data set acquisition time are key challenges for the field of whole-brain optical imaging. Combination of clearing technology and histological sectioning might provide a potential to scan deeper for each imaging-sectioning circle in the high-resolution imaging process; this is expected to further shorten the whole-brain imaging time, thereby improving whole-brain optical imaging efficiency. Current data processing of tens of TeraBytes of each data set requires powerful computing resources and have to be off-line. Exploring on-line data processing of each images of several GigaBytes during the data acquisition would yield a significant reduction in computing resource and time costs.

The ultimate goal of whole-brain optical imaging is exploration of the human brain; however, significant technical challenges exist. The mouse brain has dimensions of approximately 10 mm, whereas those of the human brain are several tens of centimeters. Thus, regardless of the employed sample preparation, whole-brain optical imaging, and image processing techniques, simple size expansion cannot be applied. Technological improvements and breakthroughs pertinent to each step are necessary. For the imaging stage in particular, if the number of field splices is simply increased, the acquisition time may be extended from a few days to several years. Therefore, development of new large-aperture optical devices, large-area array detectors, and long-range 3D scanning devices is of considerable importance to realization of high-resolution 3D human brain imaging, which will fundamentally improve

Biomedical Optics EXPRESS

the imaging throughput. In addition, development of efficient 3D optical imaging methods with the aid of computational imaging, especially machine learning and other technology, also merits attention. We believe that, with continuous breakthroughs in whole-brain optical imaging technology, the human brain will eventually be revealed.

In this review, we summarized the development of MOST in multiple contexts, including sample labeling and preparation, imaging requirements, and technological development, as well as typical brain science applications. Finally, we discussed future technological challenges. We hope this review will elucidate the field of whole-brain optical imaging and make it possible to better serve brain research as a powerful tool.

## Funding

Ministry of Science and Technology of the People's Republic of China (2015CB755602); National Natural Science Foundation of China (61721092 and 81671374).

## Acknowledgements

We are grateful to Profs. Haohong Li and Xiangning Li for valuable discussion and English writing.

## Disclosures

The authors declare no conflicts of interest.

## References

1. Q. Luo, "Brainsmatics—bridging the brain science and brain-inspired artificial intelligence," Scientia Sinica (Vitae) **47**(10), 1015 (2017).
2. L. Petreanu, T. Mao, S. M. Sternson, and K. Svoboda, "The subcellular organization of neocortical excitatory connections," Nature **457**(7233), 1142–1145 (2009).
3. J. DeFelipe, "From the Connectome to the Synaptome: An Epic Love Story," Science **330**(6008), 1198–1201 (2010).
4. T. N. Lerner, L. Ye, and K. Deisseroth, "Communication in Neural Circuits: Tools, Opportunities, and Challenges," Cell **164**(6), 1136–1150 (2016).
5. P. Rajasethupathy, E. Ferenczi, and K. Deisseroth, "Targeting Neural Circuits," Cell **165**(3), 524–534 (2016).
6. H. Zeng and J. R. Sanes, "Neuronal cell-type classification: challenges, opportunities and the path forward," Nat. Rev. Neurosci. **18**(9), 530–546 (2017).
7. M. F. Glasser, S. M. Smith, D. S. Marcus, J. L. Andersson, E. J. Auerbach, T. E. Behrens, T. S. Coalson, M. P. Harms, M. Jenkinson, S. Moeller, E. C. Robinson, S. N. Sotiropoulos, J. Xu, E. Yacoub, K. Ugurbil, and D. C. Van Essen, "The Human Connectome Project's neuroimaging approach," Nat. Neurosci. **19**(9), 1175–1187 (2016).
8. N. Kasthuri, K. J. Hayworth, D. R. Berger, R. L. Schalek, J. A. Conchello, S. Knowles-Barley, D. Lee, A. Vázquez-Reina, V. Kaynig, T. R. Jones, M. Roberts, J. L. Morgan, J. C. Tapia, H. S. Seung, W. G. Roncal, J. T. Vogelstein, R. Burns, D. L. Sussman, C. E. Priebe, H. Pfister, and J. W. Lichtman, "Saturated Reconstruction of a Volume of Neocortex," Cell **162**(3), 648–661 (2015).
9. S. W. Oh, J. A. Harris, L. Ng, B. Winslow, N. Cain, S. Mihalas, Q. Wang, C. Lau, L. Kuan, A. M. Henry, M. T. Mortrud, B. Ouellette, T. N. Nguyen, S. A. Sorensen, C. R. Slaughterbeck, W. Wakeman, Y. Li, D. Feng, A. Ho, E. Nicholas, K. E. Hirokawa, P. Bohn, K. M. Joines, H. Peng, M. J. Hawrylycz, J. W. Phillips, J. G. Hohmann, P. Wohnoutka, C. R. Gerfen, C. Koch, A. Bernard, C. Dang, A. R. Jones, and H. Zeng, "A mesoscale connectome of the mouse brain," Nature **508**(7495), 207–214 (2014).
10. T. R. Insel, S. C. Landis, and F. S. Collins; The NIH BRAIN Initiative, "Research priorities," Science **340**(6133), 687–688 (2013).
11. M. M. Poo, J. L. Du, N. Y. Ip, Z. Q. Xiong, B. Xu, and T. Tan, "China Brain Project: Basic Neuroscience, Brain Diseases, and Brain-Inspired Computing," Neuron **92**(3), 591–596 (2016).
12. H. Okano, E. Sasaki, T. Yamamori, A. Iriki, T. Shimogori, Y. Yamaguchi, K. Kasai, and A. Miyawaki, "Brain/MINDS: A Japanese National Brain Project for Marmoset Neuroscience," Neuron **92**(3), 582–590 (2016).
13. J. Mertz, "Optical sectioning microscopy with planar or structured illumination," Nat. Methods **8**(10), 811–819 (2011).
14. J.-A. Conchello and J. W. Lichtman, "Optical sectioning microscopy," Nat. Methods **2**(12), 920–931 (2005).
15. F. Helmchen and W. Denk, "Deep tissue two-photon microscopy," Nat. Methods **2**(12), 932–940 (2005).
16. W. Spalteholz, "Über das durchsichtigmachen von menschlichen und tierischen präparaten," S. Hirzel. **2**, 91 (1914).

Biomedical Optics EXPRESS


17. H. Siedentopf and R. Zsigmondy, "Uber sichtbarmachung und größenbestimmung ultramikoskopischer teilchen, mit besonderer anwendung auf goldrubingläser," Ann. Phys. **315**(1), 1–39 (1902).
18. H.-U. Dodt, U. Leischner, A. Schierloh, N. Jährling, C. P. Mauch, K. Deininger, J. M. Deussing, M. Eder, W. Zieglgänsberger, and K. Becker, "Ultramicroscopy: three-dimensional visualization of neuronal networks in the whole mouse brain," Nat. Methods **4**(4), 331–336 (2007).
19. D. S. Richardson and J. W. Lichtman, "Clarifying Tissue Clearing," Cell **162**(2), 246–257 (2015).
20. N. Renier, Z. Wu, D. J. Simon, J. Yang, P. Ariel, and M. Tessier-Lavigne, "iDISCO: a simple, rapid method to immunolabel large tissue samples for volume imaging," Cell **159**(4), 896–910 (2014).
21. C. Pan, R. Cai, F. P. Quacquarelli, A. Ghasemigharagoz, A. Lourbopoulos, P. Matryba, N. Plesnila, M. Dichgans, F. Hellal, and A. Ertürk, "Shrinkage-mediated imaging of entire organs and organisms using uDISCO," Nat. Methods **13**(10), 859–867 (2016).
22. Y. Qi, T. Yu, J. Xu, P. Wan, Y. Ma, J. Zhu, Y. Li, H. Gong, Q. Luo, and D. Zhu, "FDISCO: Advanced solvent-based clearing method for imaging whole organs," Sci. Adv. **5**, eaau8355 (2019).
23. H. Hama, H. Kurokawa, H. Kawano, R. Ando, T. Shimogori, H. Noda, K. Fukami, A. Sakaue-Sawano, and A. Miyawaki, "Scale: a chemical approach for fluorescence imaging and reconstruction of transparent mouse brain," Nat. Neurosci. **14**(11), 1481–1488 (2011).
24. A. E. Susaki, K. Tainaka, D. Perrin, F. Kishino, T. Tawara, T. M. Watanabe, C. Yokoyama, H. Onoe, M. Eguchi, S. Yamaguchi, T. Abe, H. Kiyonari, Y. Shimizu, A. Miyawaki, H. Yokota, and H. R. Ueda, "Whole-brain imaging with single-cell resolution using chemical cocktails and computational analysis," Cell **157**, 726–739 (2014).
25. K. Chung and K. Deisseroth, "CLARITY for mapping the nervous system," Nat. Methods **10**(6), 508–513 (2013).
26. K. Chung, J. Wallace, S.-Y. Kim, S. Kalyanasundaram, A. S. Andalman, T. J. Davidson, J. J. Mirzabekov, K. A. Zalocusky, J. Mattis, A. K. Denisin, S. Pak, H. Bernstein, C. Ramakrishnan, L. Grosenick, V. Gradinaru, and K. Deisseroth, "Structural and molecular interrogation of intact biological systems," Nature **497**(7449), 332–337 (2013).
27. B. Yang, J. B. Treweek, R. P. Kulkarni, B. E. Deverman, C. K. Chen, E. Lubeck, S. Shah, L. Cai, and V. Gradinaru, "Single-cell phenotyping within transparent intact tissue through whole-body clearing," Cell **158**(4), 945–958 (2014).
28. N. T. Lerner, C. Shilyansky, T. J. Davidson, K. E. Evans, K. T. Beier, K. A. Zalocusky, A. K. Crow, R. C. Malenka, L. Luo, R. Tomer, and K. Deisseroth, "Intact-Brain Analyses Reveal Distinct Information Carried by SNc Dopamine Subcircuits," Cell **162**, 635–647 (2015).
29. E. Murray, J. H. Cho, D. Goodwin, T. Ku, J. Swaney, S. Y. Kim, H. Choi, Y. G. Park, J. Y. Park, A. Hubbert, M. McCue, S. Vassallo, N. Bakh, M. P. Frosch, V. J. Wedeen, H. S. Seung, and K. Chung, "Simple, Scalable Proteomic Imaging for High-Dimensional Profiling of Intact Systems," Cell **163**(6), 1500–1514 (2015).
30. N. Renier, E. L. Adams, C. Kirst, Z. Wu, R. Azevedo, J. Kohl, A. E. Autry, L. Kadiri, K. Umadevi Venkataraju, Y. Zhou, V. X. Wang, C. Y. Tang, O. Olsen, C. Dulac, P. Osten, and M. Tessier-Lavigne, "Mapping of Brain Activity by Automated Volume Analysis of Immediate Early Genes," Cell **165**(7), 1789–1802 (2016).
31. T. Ragan, L. R. Kadiri, K. U. Venkataraju, K. Bahlmann, J. Sutin, J. Taranda, I. Arganda-Carreras, Y. Kim, H. S. Seung, and P. Osten, "Serial two-photon tomography for automated ex vivo mouse brain imaging," Nat. Methods **9**(3), 255–258 (2012).
32. K. Seiriki, A. Kasai, T. Hashimoto, W. Schulze, M. Niu, S. Yamaguchi, T. Nakazawa, K. I. Inoue, S. Uezono, M. Takada, Y. Naka, H. Igarashi, M. Tanuma, J. A. Waschek, Y. Ago, K. F. Tanaka, A. Hayata-Takano, K. Nagayasu, N. Shintani, R. Hashimoto, Y. Kunii, M. Hino, J. Matsumoto, H. Yabe, T. Nagai, K. Fujita, T. Matsuda, K. Takuma, A. Baba, and H. Hashimoto, "High-Speed and Scalable Whole-Brain Imaging in Rodents and Primates," Neuron **94**(6), 1085–1100 (2017).
33. A. Li, H. Gong, B. Zhang, Q. Wang, C. Yan, J. Wu, Q. Liu, S. Zeng, and Q. Luo, "Micro-optical sectioning tomography to obtain a high-resolution atlas of the mouse brain," Science **330**(6009), 1404–1408 (2010).
34. H. Gong, S. Zeng, C. Yan, X. Lv, Z. Yang, T. Xu, Z. Feng, W. Ding, X. Qi, A. Li, J. Wu, and Q. Luo, "Continuously tracing brain-wide long-distance axonal projections in mice at a one-micron voxel resolution," Neuroimage **74**, 87–98 (2013).
35. T. Zheng, Z. Yang, A. Li, X. Lv, Z. Zhou, X. Wang, X. Qi, S. Li, Q. Luo, H. Gong, and S. Zeng, "Visualization of brain circuits using two-photon fluorescence micro-optical sectioning tomography," Opt. Express **21**(8), 9839–9850 (2013).
36. H. Gong, D. Xu, J. Yuan, X. Li, C. Guo, J. Peng, Y. Li, L. A. Schwarz, A. Li, B. Hu, B. Xiong, Q. Sun, Y. Zhang, J. Liu, Q. Zhong, T. Xu, S. Zeng, and Q. Luo, "High-throughput dual-colour precision imaging for brain-wide connectome with cytoarchitectonic landmarks at the cellular level," Nat. Commun. **7**(1), 12142 (2016).
37. T. Jiang, B. Long, H. Gong, T. Xu, X. Li, Z. Duan, A. Li, L. Deng, Q. Zhong, X. Peng, and J. Yuan, "A platform for efficient identification of molecular phenotypes of brain-wide neural circuits," Sci. Rep. **7**(1), 13891 (2017).
38. X. Chen, X. Zhang, Q. Zhong, Q. Sun, J. Peng, H. Gong, and J. Yuan, "Simultaneous acquisition of neuronal morphology and cytoarchitecture in the same Golgi-stained brain," Biomed. Opt. Express **9**(1), 230–244 (2018).
39. M. N. Economo, N. G. Clack, L. D. Lavis, C. R. Gerfen, K. Svoboda, E. W. Myers, and J. Chandrashekar, "A platform for brain-wide imaging and reconstruction of individual neurons," eLife **5**, e10566 (2016).

Biomedical Optics EXPRESS


40. X. Li, B. Yu, Q. Sun, Y. Zhang, M. Ren, X. Zhang, A. Li, J. Yuan, L. Madisen, Q. Luo, H. Zeng, H. Gong, and Z. Qiu, "Generation of a whole-brain atlas for the cholinergic system and mesoscopic projectome analysis of basal forebrain cholinergic neurons," Proc. Natl. Acad. Sci. U.S.A. **115**(2), 415–420 (2018).
41. R. Lin, R. Wang, J. Yuan, Q. Feng, Y. Zhou, S. Zeng, M. Ren, S. Jiang, H. Ni, C. Zhou, H. Gong, and M. Luo, "Cell-type-specific and projection-specific brain-wide reconstruction of single neurons," Nat. Methods **15**(12), 1033–1036 (2018).
42. J. Peng, B. Long, J. Yuan, X. Peng, H. Ni, X. Li, H. Gong, Q. Luo, and A. Li, "A Quantitative Analysis of the Distribution of CRH Neurons in Whole Mouse Brain," Front. Neuroanat. **11**, 63 (2017).
43. C. Zhang, C. Yan, M. Ren, A. Li, T. Quan, H. Gong, and J. Yuan, "A platform for stereological quantitative analysis of the brain-wide distribution of type-specific neurons," Sci. Rep. **7**(1), 14334 (2017).
44. J. Wu, C. Guo, S. Chen, T. Jiang, Y. He, W. Ding, Z. Yang, Q. Luo, and H. Gong, "Direct 3D Analyses Reveal Barrel-Specific Vascular Distribution and Cross-Barrel Branching in the Mouse Barrel Cortex," Cereb. Cortex **26**(1), 23–31 (2016).
45. B. Xiong, A. Li, Y. Lou, S. Chen, B. Long, J. Peng, Z. Yang, T. Xu, X. Yang, X. Li, T. Jiang, Q. Luo, and H. Gong, "Precise Cerebral Vascular Atlas in Stereotaxic Coordinates of Whole Mouse Brain," Front. Neuroanat. **11**, 128 (2017).
46. C. Sotelo, "Viewing the brain through the master hand of Ramón y Cajal," Nat. Rev. Neurosci. **4**(1), 71–77 (2003).
47. H. Dong, *The Allen Reference Atlas: A Digital Color Brain Atlas of the c57bl/6j Male Mouse* (John Wiley & Sons, 2008).
48. G. Avwioro, "Histochemical uses of haematoxylin - a review," JPCS **1**, 24–34 (2011).
49. R. Gibb and B. Kolb, "A method for vibratome sectioning of Golgi-Cox stained whole rat brain," J. Neurosci. Methods **79**(1), 1–4 (1998).
50. B. Zhang, A. Li, Z. Yang, J. Wu, Q. Luo, and H. Gong, "Modified Golgi-Cox method for micrometer scale sectioning of the whole mouse brain," J. Neurosci. Methods **197**(1), 1–5 (2011).
51. Y. Choe, D. Mayerich, J. Kwon, D. E. Miller, C. Sung, J. R. Chung, T. Huffman, J. Keyser, and L. C. Abbott, "Specimen Preparation, Imaging, and Analysis Protocols for Knife-edge Scanning Microscopy," JoVE, e3248 (2011).
52. K. Amunts, C. Lepage, L. Borgeat, H. Mohlberg, T. Dickscheid, M.-É. Rousseau, S. Bludau, P.-L. Bazin, L. B. Lewis, A.-M. Oros-Peusquens, N. J. Shah, T. Lippert, K. Zilles, and A. C. Evans, "BigBrain: an ultrahigh-resolution 3D human brain model," Science **340**(6139), 1472–1475 (2013).
53. J. Wu, Y. He, Z. Yang, C. Guo, Q. Luo, W. Zhou, S. Chen, A. Li, B. Xiong, T. Jiang, and H. Gong, "3D BrainCV: Simultaneous visualization and analysis of cells and capillaries in a whole mouse brain with one-micron voxel resolution," Neuroimage **87**, 199–208 (2014).
54. U. Windhorst and H. Johansson, *Modern Techniques in Neuroscience Research* (Springer-Verlag Berlin Heidelberg, 1999).
55. J. Yuan, H. Gong, A. Li, X. Li, S. Chen, S. Zeng, and Q. Luo, "Visible rodent brain-wide networks at single-neuron resolution," Front. Neuroanat. **9**, 70 (2015).
56. D. A. Tata and B. J. Anderson, "A new method for the investigation of capillary structure," J. Neurosci. Methods **113**(2), 199–206 (2002).
57. S. Xue, H. Gong, T. Jiang, W. Luo, Y. Meng, Q. Liu, S. Chen, and A. Li, "Indian-Ink Perfusion Based Method for Reconstructing Continuous Vascular Networks in Whole Mouse Brain," PLoS One **9**(1), e88067 (2014).
58. J. Ye, L. Yang, M. R. Del Bigio, R. Summers, D. Jackson, R. L. Somorjai, T. A. Salerno, and R. Deslauriers, "Retrograde cerebral perfusion provides limited distribution of blood to the brain: A study in pigs," J. Thorac. Cardiovasc. Surg. **114**(4), 660–665 (1997).
59. D. Mayerich, J. Kwon, C. Sung, L. Abbott, J. Keyser, and Y. Choe, "Fast macro-scale transmission imaging of microvascular networks using KESM," Biomed. Opt. Express **2**(10), 2888–2896 (2011).
60. K. Miyamichi, F. Amat, F. Moussavi, C. Wang, I. Wickersham, N. R. Wall, H. Taniguchi, B. Tasic, Z. J. Huang, Z. He, E. M. Callaway, M. A. Horowitz, and L. Luo, "Cortical representations of olfactory input by trans-synaptic tracing," Nature **472**(7342), 191–196 (2011).
61. B. A. Wilt, L. D. Burns, E. T. Wei Ho, K. K. Ghosh, E. A. Mukamel, and M. J. Schnitzer, "Advances in Light Microscopy for Neuroscience," Annu. Rev. Neurosci. **32**(1), 435–506 (2009).
62. J. L. Lanciego and F. G. Wouterlood, "A half century of experimental neuroanatomical tracing," J. Chem. Neuroanat. **42**(3), 157–183 (2011).
63. Y. Luo, A. Wang, M. Liu, T. Lei, X. Zhang, Z. Gao, H. Jiang, H. Gong, and J. Yuan, "Label-free brainwide visualization of senile plaque using cryo-micro-optical sectioning tomography," Opt. Lett. **42**(21), 4247–4250 (2017).
64. B. Zingg, H. Hintiryan, L. Gou, M. Y. Song, M. Bay, M. S. Bienkowski, N. N. Foster, S. Yamashita, I. Bowman, A. W. Toga, and H. W. Dong, "Neural networks of the mouse neocortex," Cell **156**(5), 1096–1111 (2014).
65. S. Zhao, Y. Zhou, J. Gross, P. Miao, L. Qiu, D. Wang, Q. Chen, and G. Feng, "Fluorescent Labeling of Newborn Dentate Granule Cells in GAD67-GFP Transgenic Mice: A Genetic Tool for the Study of Adult Neurogenesis," PLoS One **5**(9), e12506 (2010).
66. K. Sakai and J. Miyazaki, "A transgenic mouse line that retains Cre recombinase activity in mature oocytes irrespective of the cre transgene transmission," Biochem. Biophys. Res. Commun. **237**(2), 318–324 (1997).

Biomedical Optics EXPRESS


67. H. Taniguchi, M. He, P. Wu, S. Kim, R. Paik, K. Sugino, D. Kvitsiani, Y. Fu, J. Lu, Y. Lin, G. Miyoshi, Y. Shima, G. Fishell, S. B. Nelson, and Z. J. Huang, "A resource of Cre driver lines for genetic targeting of GABAergic neurons in cerebral cortex," Neuron **71**(6), 995–1013 (2011).
68. J. Livet, T. A. Weissman, H. Kang, R. W. Draft, J. Lu, R. A. Bennis, J. R. Sanes, and J. W. Lichtman, "Transgenic strategies for combinatorial expression of fluorescent proteins in the nervous system," Nature **450**(7166), 56–62 (2007).
69. L. Luo, E. M. Callaway, and K. Svoboda, "Genetic dissection of neural circuits," Neuron **57**(5), 634–660 (2008).
70. L. Luo, E. M. Callaway, and K. Svoboda, "Genetic Dissection of Neural Circuits: A Decade of Progress," Neuron **98**(2), 256–281 (2018).
71. B. W. Banfield, J. D. Kaufman, J. A. Randall, and G. E. Pickard, "Development of pseudorabies virus strains expressing red fluorescent proteins: new tools for multisynaptic labeling applications," J. Virol. **77**(18), 10106–10112 (2003).
72. K. T. Beier, A. Saunders, I. A. Oldenburg, K. Miyamichi, N. Akhtar, L. Luo, S. P. Whelan, B. Sabatini, and C. L. Cepko, "Anterograde or retrograde transsynaptic labeling of CNS neurons with vesicular stomatitis virus vectors," Proc. Natl. Acad. Sci. U.S.A. **108**(37), 15414–15419 (2011).
73. S. J. Kuhlman and Z. J. Huang, "High-Resolution Labeling and Functional Manipulation of Specific Neuron Types in Mouse Brain by Cre-Activated Viral Gene Expression," PLoS One **3**(4), e2005 (2008).
74. I. Pollak Dorocic, D. Fürth, Y. Xuan, Y. Johansson, L. Pozzi, G. Silberberg, M. Carlén, and K. Meletis, "A whole-brain atlas of inputs to serotonergic neurons of the dorsal and median raphe nuclei," Neuron **83**(3), 663–678 (2014).
75. N. R. Wall, M. De La Parra, J. M. Sorokin, H. Taniguchi, Z. J. Huang, and E. M. Callaway, "Brain-Wide Maps of Synaptic Input to Cortical Interneurons," J. Neurosci. **36**(14), 4000–4009 (2016).
76. A. Wang, J. Yuan, W. Luo, M. Liu, and Q. Luo, "Optimization of sample cooling temperature for redox cryo-imaging," J. Biomed. Opt. **19**(8), 080502 (2014).
77. H. M. Lai, A. K. L. Liu, H. H. M. Ng, M. H. Goldfinger, T. W. Chau, J. DeFelice, B. S. Tilley, W. M. Wong, W. Wu, and S. M. Gentleman, "Next generation histology methods for three-dimensional imaging of fresh and archival human brain tissues," Nat. Commun. **9**(1), 1066 (2018).
78. D. Wang, C. R. Stockard, L. Harkins, P. Lott, C. Salih, K. Yuan, D. Buchsbaum, A. Hashim, M. Zayzafoon, R. W. Hardy, O. Hameed, W. Grizzle, and G. P. Siegal, "Immunohistochemistry in the evaluation of neovascularization in tumor xenografts," Biotech. Histochem. **83**(3-4), 179–189 (2008).
79. X. Yao, C. N. Qian, Z. F. Zhang, M. H. Tan, E. J. Kort, X. J. Yang, J. H. Resau, and B. T. Teh, "Two distinct types of blood vessels in clear cell renal cell carcinoma have contrasting prognostic implications," Clin. Cancer Res. **13**(1), 161–169 (2007).
80. T. C. Murakami, T. Mano, S. Saikawa, S. A. Horiguchi, D. Shigeta, K. Baba, H. Sekiya, Y. Shimizu, K. F. Tanaka, H. Kiyonari, M. Iino, H. Mochizuki, K. Tainaka, and H. R. Ueda, "A three-dimensional single-cell-resolution whole-brain atlas using CUBIC-X expansion microscopy and tissue clearing," Nat. Neurosci. **21**(4), 625–637 (2018).
81. E. A. Susaki, K. Tainaka, D. Perrin, H. Yukinaga, A. Kuno, and H. R. Ueda, "Advanced CUBIC protocols for whole-brain and whole-body clearing and imaging," Nat. Protoc. **10**(11), 1709–1727 (2015).
82. A. Ertürk, K. Becker, N. Jährling, C. P. Mauch, C. D. Hojer, J. G. Egen, F. Hellal, F. Bradke, M. Sheng, and H.-U. Dodt, "Three-dimensional imaging of solvent-cleared organs using 3DISCO," Nat. Protoc. **7**(11), 1983–1995 (2012).
83. K. Tainaka, S. I. Kubota, T. Q. Suyama, E. A. Susaki, D. Perrin, M. Ukai-Tadenuma, H. Ukai, and H. R. Ueda, "Whole-Body Imaging with Single-Cell Resolution by Tissue Decolorization," Cell **159**(4), 911–924 (2014).
84. I. Begemann and M. Galic, "Correlative Light Electron Microscopy: Connecting Synaptic Structure and Function," Front. Synaptic Neurosci. **8**, 28 (2016).
85. S. Mikula and W. Denk, "High-resolution whole-brain staining for electron microscopic circuit reconstruction," Nat. Methods **12**(6), 541–546 (2015).
86. M. Belle, D. Godefroy, G. Couly, S. A. Malone, F. Collier, P. Giacobini, and A. Chedotal, "Tridimensional Visualization and Analysis of Early Human Development," Cell **169**, 161–173 (2017).
87. K. L. Kusser and T. D. Randall, "Simultaneous detection of EGFP and cell surface markers by fluorescence microscopy in lymphoid tissues," J. Histochem. Cytochem. **51**(1), 5–14 (2003).
88. E. Brown and P. Verkade, "The use of markers for correlative light electron microscopy," Protoplasma **244**(1-4), 91–97 (2010).
89. T. Kasuya, T. Yamada, A. Uyeda, T. Matsuzaki, T. Okajima, K. Tatematsu, K. Tanizawa, and S. Kuroda, "In vivo protein delivery to human liver-derived cells using hepatitis B virus envelope pre-S region," J. Biosci. Bioeng. **106**(1), 99–102 (2008).
90. K. Ninomiya, K. Noda, C. Ogino, S. Kuroda, and N. Shimizu, "Enhanced OH radical generation by dual-frequency ultrasound with TiO2 nanoparticles: Its application to targeted sonodynamic therapy," Ultrason. Sonochem. **21**(1), 289–294 (2014).
91. L. Schoonen and J. C. M. van Hest, "Functionalization of protein-based nanocages for drug delivery applications," Nanoscale **6**(13), 7124–7141 (2014).
92. D. R. Keene, S. F. Tufa, G. P. Lunstrum, P. Holden, and W. A. Horton, "Confocal/TEM Overlay Microscopy: A Simple Method for Correlating Confocal and Electron Microscopy of Cells Expressing GFP/YFP Fusion Proteins," Microsc. Microanal. **14**(4), 342–348 (2008).

Biomedical Optics EXPRESS


93. K. Choudhuri, J. Llodrá, E. W. Roth, J. Tsai, S. Gordo, K. W. Wucherpfennig, L. C. Kam, D. L. Stokes, and M. L. Dustin, "Polarized release of T-cell-receptor-enriched microvesicles at the immunological synapse," Nature **507**(7490), 118–123 (2014).
94. J. Yao, A. A. Kaberniuk, L. Li, D. M. Shcherbakova, R. Zhang, L. Wang, G. Li, V. V. Verkhusha, and L. V. Wang, "Multiscale photoacoustic tomography using reversibly switchable bacterial phytochrome as a near-infrared photochromic probe," Nat. Methods **13**(1), 67–73 (2016).
95. I. Walter, M. Fleischmann, D. Klein, M. Müller, B. Salmons, W. H. Günzburg, M. Renner, and W. Gelbmann, "Rapid and Sensitive Detection of Enhanced Green Fluorescent Protein Expression in Paraffin Sections by Confocal Laser Scanning Microscopy," Histochem. J. **32**(2), 99–103 (2000).
96. X. Jiang, Z. Kalajzic, P. Maye, A. Braut, J. Bellizzi, M. Mina, and D. W. Rowe, "Histological Analysis of GFP Expression in Murine Bone," J. Histochem. Cytochem. **53**(5), 593–602 (2005).
97. Y. Kfoury and D. T. Scadden, "Mesenchymal cell contributions to the stem cell niche," Cell Stem Cell **16**(3), 239–253 (2015).
98. S. B. Newman, E. Borysko, and M. Swerdlow, "New Sectioning Techniques for Light and Electron Microscopy," Science **110**(2846), 66–68 (1949).
99. Q. Wang, A. Li, H. Gong, D. Xu, and Q. Luo, "Quantitative study on the hygroscopic expansion of spurr resin to obtain a high-resolution atlas of the mouse brain," Exp. Biol. Med. (Maywood) **237**(10), 1134–1141 (2012).
100. P. Osten and T. W. Margrie, "Mapping brain circuitry with a light microscope," Nat. Methods **10**(6), 515–523 (2013).
101. X. Wang, J. Tucciarone, S. Jiang, F. Yin, B.-s. Wang, D. Wang, Y. Jia, X. Jia, Y. Li, T. Yang, Z. Xu, M. A. Akram, Y. Wang, S. Zeng, G. A. Ascoli, P. Mitra, H. Gong, Q. Luo, and J. Z. Huang, "Genetic single neuron anatomy reveals fine granularity of cortical axo-axonic cells," Cell Rep. **26**, 3145–3159e3145 (2019).
102. R. Cai, C. Pan, A. Ghasemigharagoz, M. I. Todorov, B. Förstera, S. Zhao, H. S. Bhatia, A. Parra-Damas, L. Mrowka, D. Theodorou, M. Rempfler, A. L. R. Xavier, B. T. Kress, C. Benakis, H. Steinke, S. Liebscher, I. Bechmann, A. Liesz, B. Menze, M. Kerschensteiner, M. Nedergaard, and A. Ertürk, "Panoptic imaging of transparent mice reveals whole-body neuronal projections and skull-meninges connections," Nat. Neurosci. **22**(2), 317–327 (2019).
103. X. Yang, Q. Zhang, F. Huang, K. Bai, Y. Guo, Y. Zhang, N. Li, Y. Cui, P. Sun, S. Zeng, and X. Lv, "High-throughput light sheet tomography platform for automated fast imaging of whole mouse brain," J. Biophotonics **11**(9), e201800047 (2018).
104. J. W. Lichtman and W. Denk, "The big and the small: challenges of imaging the brain's circuits," Science **334**(6056), 618–623 (2011).
105. K. D. Micheva and S. J. Smith, "Array Tomography: A New Tool for Imaging the Molecular Architecture and Ultrastructure of Neural Circuits," Neuron **55**(1), 25–36 (2007).
106. F. Zhu, M. Cizeron, Z. Qiu, R. Benavides-Piccione, M. V. Kopanitsa, N. G. Skene, B. Koniaris, J. DeFelipe, E. Fransén, N. H. Komiyama, and S. G. N. Grant, "Architecture of the Mouse Brain Synaptome," Neuron **99**(4), 781–799 (2018).
107. Y. Kim, G. R. Yang, K. Pradhan, K. U. Venkataraju, M. Bota, L. C. García Del Molino, G. Fitzgerald, K. Ram, M. He, J. M. Levine, P. Mitra, Z. J. Huang, X.-J. Wang, and P. Osten, "Brain-wide Maps Reveal Stereotyped Cell-Type-Based Cortical Architecture and Subcortical Sexual Dimorphism," Cell **171**(2), 456–469 (2017).
108. D. Mayerich, L. Abbott, and B. McCormick, "Knife-edge scanning microscopy for imaging and reconstruction of three-dimensional anatomical structures of the mouse brain," J. Microsc. **231**(Pt 1), 134–143 (2008).
109. Y. Sun, H. Yu, D. Zheng, Q. Cao, Y. Wang, D. Harris, and Y. Wang, "Sudan black b reduces autofluorescence in murine renal tissue," Arch. Pathol. Lab. Med. **135**(10), 1335–1342 (2011).
110. V. C. Oliveira, R. C. Carrara, D. L. Simoes, F. P. Saggioro, C. G. Carlotti, Jr., D. T. Covas, and L. Neder, "Sudan Black B treatment reduces autofluorescence and improves resolution of in situ hybridization specific fluorescent signals of brain sections," Histol. Histopathol. **25**(8), 1017–1024 (2010).
111. T. Quan, T. Zheng, Z. Yang, W. Ding, S. Li, J. Li, H. Zhou, Q. Luo, H. Gong, and S. Zeng, "NeuroGPS: automated localization of neurons for brain circuits using L1 minimization model," Sci. Rep. **3**(1), 1414 (2013).
112. S. K. Baisley, C. L. Cloninger, and V. P. Bakshi, "Fos expression following regimens of predator stress versus footshock that differentially affect prepulse inhibition in rats," Physiol. Behav. **104**(5), 796–803 (2011).
113. J. D. Whitesell, A. R. Buckley, J. E. Knox, L. Kuan, N. Graddis, A. Pelos, A. Mukora, W. Wakeman, P. Bohn, A. Ho, K. E. Hirokawa, and J. A. Harris, "Whole brain imaging reveals distinct spatial patterns of amyloid beta deposition in three mouse models of Alzheimer's disease," J. Comp. Neurol. **527**, 1–24 (2018).